Bulletin of the Seismological Society of America, Vol. 68, No. 2, pp. 283–300, April, 1978

THE INFLUENCE OF RUPTURE INCOHERENCE ON SEISMIC DIRECTIVITY

BY DAVID M. BOORE AND WILLIAM B. JOYNER

ABSTRACT

As has long been recognized in teleseismic studies, smooth rupture propagation significantly modifies the azimuthal variation in elastic wave radiation and introduces a dependence of peak motion on the ratio of rupture velocity to wave propagation velocity. Rupture propagation also has a first-order effect on the ground motions close to faults as calculated from models of coherent rupture. For engineering purposes, it is important to know whether the effect occurs only with coherent ruptures, or whether it is a more general phenomena of propagating faults. This question was examined by both analytical and Monte Carlo studies of models of nonuniform ruptures. The principal models were defined by ruptures moving continuously in time along the fault with random variations in rupture velocity or in slip amplitude. These models were richer in high frequencies than the corresponding smooth ruptures. The randomness introduced a new corner into the spectrum at a frequency that is simply related to the coherence length of the random variations and to the azimuth between the fault and station. The lower frequency corner due to the overall rupture was preserved. For the model with varying rupture velocity the azimuthal variation in spectral amplitude was enhanced over that for the smooth rupture. For the model with varying slip the azimuthal variation was the same as for a smooth rupture. These models showed directivity effects as strong or stronger than the corresponding smooth rupture, providing that the average rupture velocity was the same. Monte Carlo simulations with statistical models gave peak amplitudes with the same general dependence on rupture velocity as the peak amplitudes from smooth ruptures although in the mean the peak motions were enhanced in the incoherent model. An analytic expression was also derived for the mean spectrum of an extreme model in which rupture occurred in little patches distributed with complete randomness over the fault surface and in time. Even this model showed some effects of directivity. The results of our study are consistent with the interpretation that rupture propagation produces destructive interference in the radiated motion; incoherence reduces this interference and in general leads to higher peak motions and spectral levels.

INTRODUCTION

Smooth-rupture propagation can lead both to large azimuthal differences in the radiation of elastic energy and to significant sensitivity of peak motions to the ratio of rupture velocity and wave propagation velocity. Although this has long been recognized in applications at teleseismic distances (e.g., Benioff, 1955), the implications for the computation of ground motion close to faults are not as widely recognized, although the same directivity effects should be expected (and have been observed in model studies; see Archuleta and Brune, 1975). In fact, these effects can be so large that one wonders if they exist in the real world. For example, Figures 1 and 2, taken from a study concerning ground motions from the 1906 San Francisco earthquake (Boore, 1977), show a factor of 4 increase in computed ground motions around 5-sec period for a change of rupture velocity from 2 to 3 km/sec, and a 13:1 ratio in the peak motions expected ahead of and behind the rupture. Clearly these results, if real, constitute a first-order effect on the computations of design motions close to faults.

It is our feeling that such effects are held by many seismologists and earthquake engineers to be unrealistic, although there are few good data to test the predictions. Usually, appeals are made to incoherence of both the fault process and the wave propagation to reduce these effects. The presence of such incoherence is very reasonable, especially at the short wavelengths of interest to earthquake engineers.

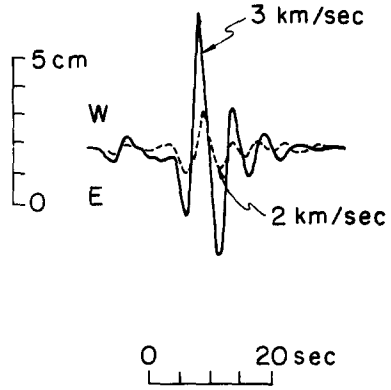

FIG. 1. Theoretical body-wave recordings at Lick Observatory from a model of the 1906 earthquake on the San Andreas fault. The closest point of rupture and the shear velocity were 35 km and 3.3 km/sec, respectively (adapted from Figure 8 in Boore, 1977; see Figure 1 in that paper for the geometry). Both near- and far-field terms were included in the calculations, but the near-field terms contributed little to the motion at these frequencies.

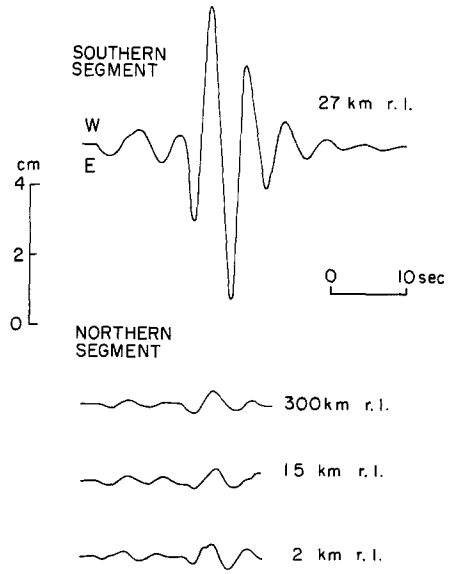

FIG. 2. Body waves from the same faulting used in the computations of Figure 1, showing the separate contributions of the segments to the north and south of the epicenter off the Golden Gate, near San Francisco. The total dislocation on each segment was the same. The stopping phases from the northern segment are not shown, but are smaller than the motions illustrated. r. l. stands for rupture length.

Our aim is to study the effect of such incoherence on the radiated motion. This study differs in several essential ways from previous work dealing with variable rupture properties. We are concerned with the azimuthal variation of ground-motion amplitude and thus do not average over azimuth, as was done by Haskell (1964, 1966) and Blandford (1975). Furthermore, we introduce the randomness into the model in a more physical way than did Aki (1967, 1972) or Haskell (1964, 1966), who specified autocorrelation functions.

We start by reviewing the effects of smooth rupture. This serves as a basis of comparison for the main part of the paper in which the expected value of the radiation from nonuniform faults is computed both analytically and from Monte Carlo simulation. Most of the analysis is concerned with unilaterally propagating faults along which the slip and rupture velocity vary according to some probability distribution. For such a fault randomness is superposed on a uniformly propagating rupture. We also give brief consideration to radiation from a fault in which slip can occur at any time with equal probability at any point on the fault; this is the most random rupture we can imagine.

Effect of Rupture Propagation: Review

Before describing our statistical model, it is useful to review the basic effects of smooth rupture propagation. In an infinite uniform, isotropic and elastic medium, the displacement from a small rectangular fault in which rupture starts at one end and propagates smoothly is given by

$$u = \frac{R(\theta, \phi)}{4\pi\rho c^3}\frac{M_0}{r}\left\{\frac{\dot{D}(t)}{D_0} * \frac{B(t; \Delta t_L)}{\Delta t_L} * \frac{B(t; \Delta t_W)}{\Delta t_W}\right\} \tag{1}$$

in which u is a given component of the P or S wave (according to the choice of the material velocity c and the radiation pattern $R(\theta, \phi)$), r is an average distance between the fault and station, M_0 is the static moment ($= \mu D_0 L W$), $D(t)$ is the source time function, with static amplitude D_0 (assumed to be constant over the fault surface), ρ is density, and $B(t; \Delta t)$ is a boxcar function of duration Δt and unit height; the duration Δt_L and Δt_W are the differences in arrival times for energy coming from either end of the fault (Δt_L) or from the upper and lower edges (Δt_W), assuming a step source time function, and the symbol $*$ is the convolution operator. (See Savage, 1971; Geller, 1976; for a better model of an extended rupture see Savage, 1966 and the comments in Boore and Stierman, 1976.) We have neglected near-field terms in the equation above and have assumed that the source dimensions are small compared to r.

In order to isolate the effect of rupture propagation, we consider (1) SH motion only, in the orthogonal plane bisecting the fault along its length and (2) a step source time function. For a narrow fault and at distances several fault lengths away

$$\Delta t_L = L\left(\frac{1}{V} - \frac{\cos\theta}{\beta}\right) \tag{2}$$

and equation (1) simplifies to

$$u(t) = \frac{\cos 2\theta}{4\pi\rho\beta^3}\frac{M_0}{r}\frac{B(t, \Delta t_L)}{\Delta t_L}. \tag{3}$$

θ is the angle between the strike of the fault and the line connecting the epicenter and the observation points. If the waves propagate out of the perpendicular bisecting plane of the fault, the cos θ/β term in equation (2) should be replaced by the apparent slowness of the wave in the direction of rupture propagation. This can reduce the effective Mach number, particularly for teleseismic body waves from vertical faults.

The Fourier amplitude spectrum of $u(t)$ is given by

$$U(\omega) = \frac{|\cos 2\theta|}{4\pi\rho\beta^3}\frac{M_0}{r}\frac{|\sin \omega\Delta t_L/2|}{|\omega\Delta t_L/2|}. \tag{4}$$

In the discussion below, the point source radiation pattern, $|\cos 2\theta|$, will be ignored, leaving azimuthal variations only in the dependence of Δt_L on θ. The envelope of the spectrum is sketched in Figure 3 for several θ's and several Mach numbers (V/β = Mach number). As is well known, the effect of rupture is to produce destructive interference and therefore reduce the high-frequency motions by introducing a ω^{-1} roll-off beyond a corner frequency which depends on θ and V/β. An upper bound to the spectra is given by radiation from a point source with the same moment, for then $\Delta t_L \cong 0$ and the radiation will be an impulse with a flat spectrum. For extended ruptures, a flat spectrum is produced at particular azimuths for supersonic Mach numbers ($\theta = 0°$ for $V/\beta = 1$ and $\theta = 90°$ for $V/\beta = \infty$).

For a given M_0, the output of an instrument whose high frequency cutoff is at frequencies lower than the corner frequency will not depend on rupture velocity or θ (in effect, the ground displacement looks like an impulse). On the other hand, the propagation effect will produce significant azimuthal variations and sensitivity

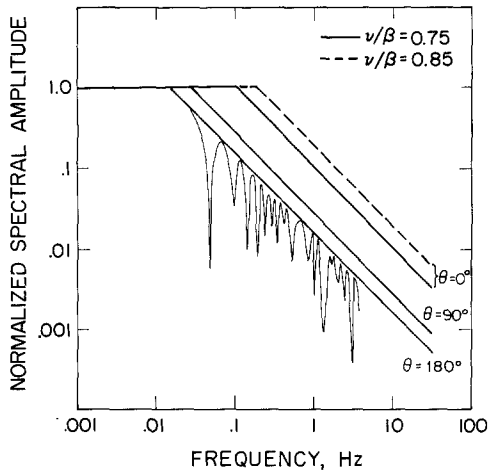

FIG. 3. The effects of directivity on the seismic spectrum, showing the variations with azimuth and Mach number. The lines shown are the spectral envelopes formed from the low- and high-frequency asymptotes.

of the amplitude to Mach number in the output from higher frequency instruments. Note that Δt_L and M_0 are both proportional to L, and therefore the amplitude of the ground displacement will not depend on the fault length. This explains why the peak amplitudes in the seismograms in Figure 2 are virtually identical for fault lengths ranging from 300 to 2 km. (In this case the corner frequency associated with even the 2-km rupture is less than the resonant frequency of the 5 sec, underdamped instrument.)

The rupture factor which controls the amplitude is plotted in Figure 4. From this we see that the azimuthal and Mach number sensitivity of the amplitudes is most pronounced for azimuths in the direction of rupture propagation. The effect of rupture propagation is often referred to as directivity (Ben-Menahem, 1961) and is sometimes described as focusing energy in the direction of rupture propagation. This can be misleading, for compared with radiation from a point source with the same moment, the waves from an extended rupture are always smaller in both the amplitude and frequency domain. Rather than focusing, the effect of rupture is to produce destructive interference. The destructive interference is greater at back

azimuths, however, and thus it appears that energy is being focused on a forward direction.

INCOHERENT RUPTURE

The statistical model. What is the effect of nonuniform rupture? From the discussion above, there will be less destructive interference and, in general, the amplitudes of the waves, especially at high frequencies, will be increased at all azimuths. To study these effects quantitatively, we model the rupture as unidirectional propagation along a fault subdivided into segments which are triggered sequentially by the rupture front. Each segment corresponds to the idealized model of the previous section, with the length, total slip, and rupture velocity for each segment (l, d, and v, respectively) chosen statistically from probability density functions. (Lower case letters represent segment parameters; upper case letters correspond to parameters for the whole fault.) The rupture moves continuously in

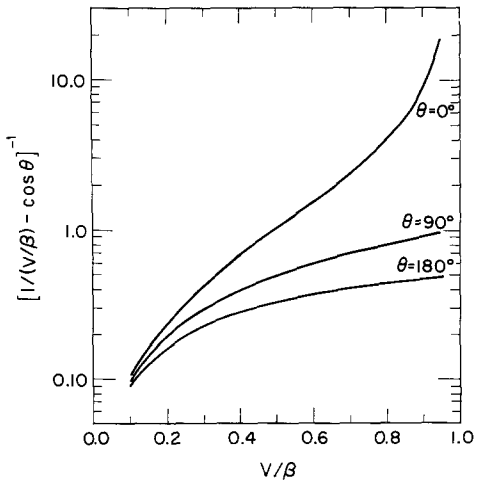

FIG. 4. The dependence of the directivity on Mach number and azimuth. The peak motions are proportional to the ordinate. Note the disproportionate change going from azimuths of 0° to 90° compared to that from 90° to 180°.

time along the fault. To isolate the rupture effect, we assumed constant width, W, and a step source time function. From this description, it is easy to do computer Monte Carlo simulations of the waves from this fault, using a random number generator. It is also possible to find an expression for the mean spectra, averaged over the ensemble. Both approaches have been used here.

Lacking information to the contrary, for simplicity the probability density functions for the rupture velocity and dislocation have been taken as rectangular distributions. More generality could be obtained by using the β distribution (Ang and Tang, 1975, p. 129). The probability function for segment lengths was assumed to be an exponential distribution, with a mean length $\bar{l}$. With that assumption, the occurrence of transitions from one fault segment to the next is governed by a Poisson distribution, and the process is highly irregular.

In common with other dislocation models, our source is unrealistic because of the presence of stress singularities. We could impose a smoothness constraint on the dislocation amplitudes to guarantee nonsingular stresses. Doing this would probably not influence the general conclusions of this paper, however, and therefore

we have kept the simple model. Das and Aki (1977) have studied the radiation from a model in which stresses vary along the fault, and some of the features they see, such as increased high frequencies, especially in the forward azimuths, and insensitivity of the low frequency corner to the statistical variations, agree with our findings.

It is interesting to note that the variation of rupture velocity we have chosen is consistent with some recent ideas concerning source mechanics. Madariaga (1977) points out that a sudden change in rupture velocity is expected whenever a rapid change in the strength of the fault is encountered. Furthermore, Nur (1978) argues that frictional stresses vary along rupture surfaces with a statistical distribution similar to the one we have used for our segment lengths.

Mean spectra. We have chosen to concentrate on the spectra of the waves rather than the peak motions. This is both because the peak motions are usually a function of instrument type and thus only provide information about a narrow frequency band and because it is easy to study the expected value of the spectra using established statistical techniques.

Although the Monte Carlo approach above is an easy way to generate a suite of ground motions, it is a cumbersome way of studying the statistical mean of the process. In our case we are able to derive an analytic formula for the mean spectrum corresponding to an approximation of the statistical model described above. The time series from the statistical model will be a series of adjacent box functions as shown in Figure 5. With the assumption that the amplitudes of adjacent boxes are statistically independent, that the duration of each box is given by an exponential probability distribution, and that the average duration of each box is short compared to the overall duration of faulting as seen at the receiving station, the mean spectra, $\bar{U}$, of the process is given by

$$\bar{U}(\omega) = \frac{|\cos 2\theta|}{4\pi\rho\beta^3} \frac{\bar{M}_0}{r} (\bar{E})^{1/2} \tag{5}$$

where

$$\bar{E} = \frac{\sin^2(\omega\Delta t_L/2)}{(\omega\Delta t_L/2)^2} + 2\left(\frac{\sigma_a}{\bar{a}}\right)^2 \left(\frac{\bar{t}}{\Delta t_L}\right) \left[\frac{1}{1 + (\omega\bar{t})^2}\right]. \tag{6}$$

(See Appendix A for the derivation of this and a more general expression.) In the equation, $\bar{a}$ and σ_a are proportional to the mean and standard deviation of the amplitudes, respectively, and $\bar{t}$ is the mean duration of the box functions in Figure 5. Δt_L is the overall duration of faulting, as given by equation (2). The moment $\bar{M}_0$ is defined later.

The equation for $\bar{E}$ shows that the mean spectrum is the sum of a deterministic part [compare the first term with equation (4)] and a statistical part. This is in keeping with our fault model, which is deterministic in the sense that it is a unilateral rupture with a given average length and average rupture velocity. Both terms approach constant values at low frequency, and decay as ω^{-1} at high frequencies. The corner of the random part of the spectrum is at a higher frequency than that from the deterministic part, and if the condition

$$\left(\frac{\sigma_a}{\bar{a}}\right)^2 \left(\frac{\Delta t_L}{\bar{t}}\right) \geqq 2 \tag{7}$$

is satisfied, the random part of the spectrum will dominate at high frequencies. The result is an enrichment of high frequencies and the appearance of two spectral corners; one associated with the rupture over the whole fault length at the mean velocity, and the other, at higher frequencies, related to rupture over the coherence length $\bar{l}$. It is the preservation of the lower frequency corner associated with rupture over the whole fault that makes our spectra different than that of Aki (1967, 1972) and Haskell (1964, 1966). The effect of the two corners is to introduce a spectral decay with intermediate slope between the ω^0 and ω^{-1} low- and high-frequency asymptotes. With our assumption that the coherence length is significantly smaller than the fault length, the low-frequency limit of $\bar{E}$ is unity and the spectrum approaches that of a smooth, coherent rupture.

To illustrate the effects of statistical variations in fault parameters, we must specify the azimuthally dependent quantities $\bar{a}$, σ_a, and $\bar{t}$ [Δt_L is given by equation (2)] in terms of the statistics of the slip, rupture velocity, and segment lengths of

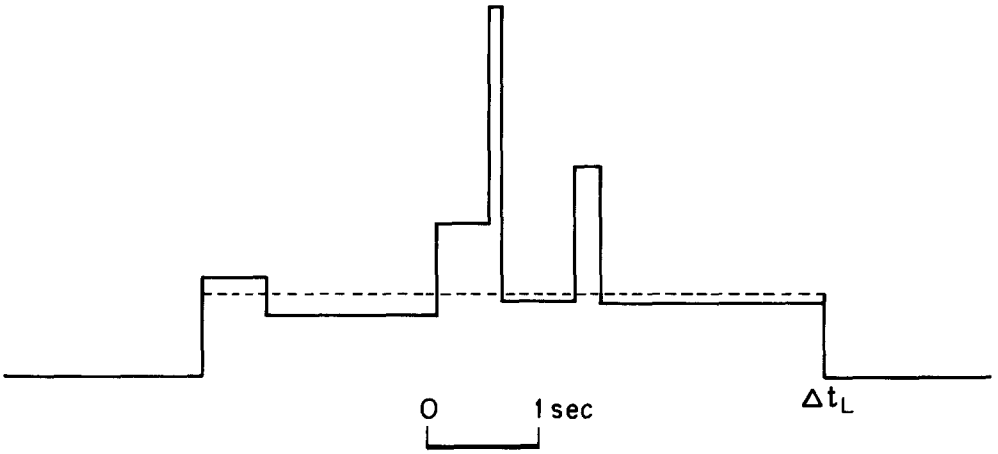

FIG. 5. A typical ground displacement wave form for the incoherent model of rupture discussed in the text. The dashed line is the correponding wave form for a smooth rupture with the same moment.

the fault. The equations connecting the fault parameters and the ground parameters, for the ith fault segment, can be found from equations (2) and (3)

$$a_i = d_i(1/v_i - \cos\theta/\beta)^{-1} \tag{8a}$$

$$t_i = l_i(1/v_i - \cos\theta/\beta). \tag{8b}$$

Since d, l, and v are random variables so are a and t, and the expected values of the ground-motion parameters $\bar{a}$, σ_a, $\bar{t}$ can be determined using the equations above and the statistics of the fault parameters (because of the independence of parameters from segment to segment of the fault, we have dropped the subscript i). For example

$$\bar{t} = \left[\int \lambda p_l(\lambda)d\lambda\right]\left[\int \left(\frac{1}{v} - \frac{\cos\theta}{\beta}\right) p_v(v)dv\right] \tag{9}$$

where p_l, p_v are the probability density functions of the segment length and rupture velocity, respectively (Ang and Tang, 1975, p. 196). For our assumed rectangular distributions for v and d, and the exponential distribution for l, it is easy to evaluate

the integrals and obtain analytic expressions for $\bar{a}$, σ_a, and $\bar{t}$ which have as parameters the upper and lower limits of fault slip and rupture velocity, the mean coherence length, and the azimuth from the fault strike. Much of the effect of the random fluctuations in the fault parameters can be understood by studying $\bar{a}$, σ_a, and $\bar{t}$ directly, even though these quantities were introduced in an intermediate step in the evaluation of the mean spectrum. We have chosen to isolate the cases of constant rupture velocity and variable slip, and variable rupture velocity and constant slip. In each case the mean rupture velocity was taken as 2.5 km/sec (compared to a shear velocity of 3.3 km/sec), the mean slip was 1.0 unit, and the mean coherence length was 1 km. The overall fault length was 30 km. Figure 6 shows the results as a function of azimuth. For comparison, the smooth rupture without statistical fluctuations predicts the same $\bar{a}$ as the case of constant rupture velocity and variable slip. For variable slip, the ratio $\sigma_a/\bar{a}$ does not decrease with azimuth, and we would predict from equation (5) that the high-frequency spectral levels would be increased at all azimuths relative to the case of smooth rupture. In contrast is the expected behavior for variable rupture velocity and constant slip. For most azimuths, $\sigma_a/\bar{a}$ is small and therefore the statistical variations in fault properties will have a minor effect on the mean spectrum. It is only for angles near $\theta = 0°$ that $\sigma_a/\bar{a}$ is large, and therefore the mean spectra will be increased at these azimuths compared with a smooth rupture. In this case, then, the effects of directivity will be enhanced compared to a coherent rupture. Another effect predictable from Figure 6 is the relative smoothness of the mean spectra. The presence of incoherence leads to shifting spectral holes in the individual members of the statistical ensemble. In general, the greater the incoherence, the more shifting of holes, and the smoother the resulting mean spectrum. Thus, at azimuths away from 0° we would expect the mean spectra for the case of variable rupture velocity to be more jagged than those due to variable slip. On the other hand, the opposite should be true for azimuths close to 0°, where σ_a for the variable rupture velocity case increases rapidly.

In Figures 7, 8, and 9 we show mean spectra that illustrate some of the comments made above. Figure 7 shows the spectra at forward and back azimuths ($\theta = 0°$ and 180°). The predictions about relative smoothness are clearly borne out, as are the expected azimuthal differences. Note that the spectra for the variable slip, constant rupture velocity case are increased relative to smooth rupture by about the same factor at both azimuths. In contrast, the variable rupture velocity case leads to a large increase in directivity. This is seen more clearly in Figure 8, which shows the spectra for the three cases at azimuths of 0°, 90°, and 180°. From this we can say that rather than reduce the effects of directivity, random variation of fault parameters may enhance the azimuthal variations of the mean spectra from a unidirectional fault.

The effects of coherence length are shown in Figure 9. As expected, the spectral corner and thus the high frequency energy increases with decreasing coherence length, with a flattening of the spectrum between the corners associated with the overall rupture length ($f = 0.11$ Hz) and the coherence length ($f = 0.3$, 1.4, 2.9 Hz for $\bar{l} = 5.0$, 1.0, 0.5, respectively).

There are two problems with our derivation of the mean spectrum for the case of variable rupture velocity. The first is that although we assumed an exponential distribution for t, equation (8b) shows that the probability density function for t will be a combination of an exponential distribution for l and a rectangular distribution for v. The mean and standard deviation of an exponential distribution are equal,

but Figure 6 shows that σ_t and $\bar{t}$ may differ by 40 per cent for the cases considered here. Statistical tests, however, show that for our purposes the assumption of an exponential distribution isn't too bad, especially if we use the mean of $\bar{t}$ and $\bar{\sigma}_t$ in place of $\bar{t}$ in equation (6).

The second problem with the formula for the mean spectrum when variable rupture velocity is allowed is related to the low frequency limit. For any given member of the ensemble we expect the low frequency limit of the spectrum to be independent of azimuth and rupture velocity (ignoring radiation pattern terms) and to be proportional to the moment $M_0 = \mu \bar{d}\, LW$. Thus, the ensemble average should have the same property. In our equation (5) this isn't the case. The main reason for this is that the amplitude, a, and duration, t, of each box are assumed to

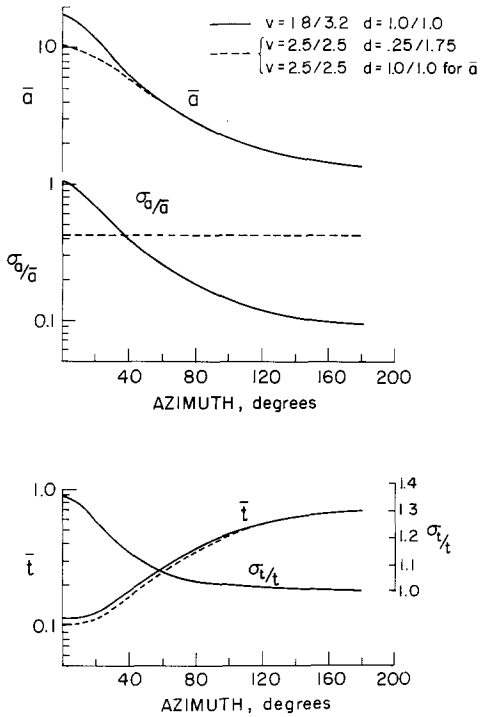

FIG. 6. Azimuthal variation of the mean height and duration of the square waves of Figure 5, and their standard deviations, for the statistical models shown in the legend. The numbers separated by a slash in the legend refer to the upper and lower bounds of the random variables rupture velocity (v) and dislocation (d). The mean coherence length was taken as 1 km and the total fault length was 30 km.

be independent, although their product should equal $d\bar{l}$. Treating a and t as independent statistical variables, however, means that the directivity terms involving rupture velocity ($1/v - \cos\theta/\beta$) will not cancel [see equations (8a) and (8b)] and the product is then a function of azimuth and rupture velocity. Because of this, the mean moment in equation (5), defined as

$$\bar{M}_0 = \mu W(L/\bar{l})\bar{a}\bar{t} \tag{10}$$

will depend on azimuth and rupture velocity. In the results here, we normalize the spectra to unity at zero frequency to avoid this second problem. In the case where velocity is constant but slip varies, neither of the problems arise, and equations (5) and (6) hold without qualification.

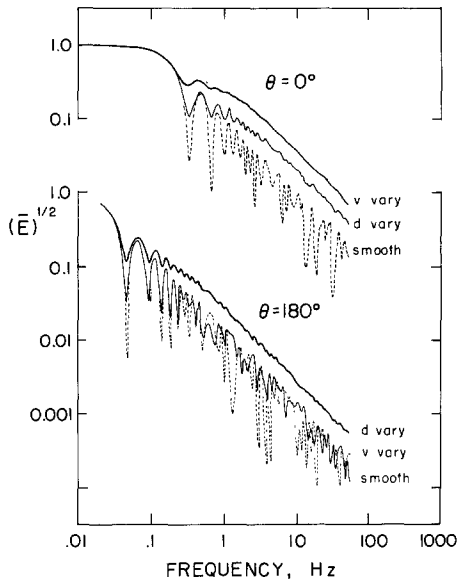

FIG. 7. The mean spectra calculated from equation (A4) for forward and back azimuths and three types of faulting: smooth, coherent faulting with 2.5 km/sec rupture velocity and fault slip of 1.0 units; variable rupture velocity (v vary) with upper and lower limits of 3.2 and 1.8 km/sec, respectively; and variable fault slip (d vary) between limits of 0.25 and 1.75 units. In the latter two cases the mean of the fault properties was the same as for the smooth rupture. Rupture length was 30 km and coherence length was 1.0 km. A shear velocity of 3.3 km/sec was assumed. Ordinate is in arbitrary units.

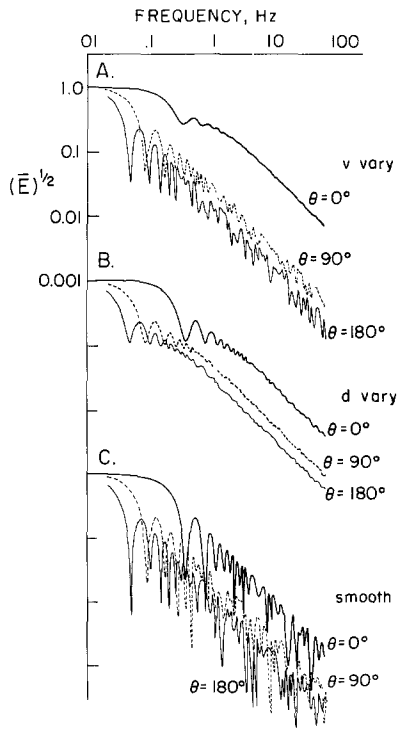

FIG. 8. Similar to Figure 7, but showing the directivity effect for each type of randomness separately.

To assess the importance of the limitations just described, a Monte Carlo computer simulation was performed. Twenty spectra were generated, and the square root of the mean square amplitude spectrum was formed at each frequency to compare with the analytic results. The case of constant rupture velocity, variable slip was first simulated to check the basic derivation of equation (5) and the ability of the Monte Carlo technique to give reliable mean spectra based on 20 ensemble members. The results, shown in Figure 10, are sufficiently close to the analytical results for us to be confident of our method. As an aside, note the scrambling of spectral holes. Hanks (1972) noted this in a similar study and pointed out the difficulty of using such holes to infer rupture parameters (the corner frequency seems to be a more stable parameter).

The simulation of the constant slip, variable rupture velocity case is shown in Figure 11. Nearly identical results were obtained from another simulation with a different seed for the random number generator. Clearly, the analytical formula is

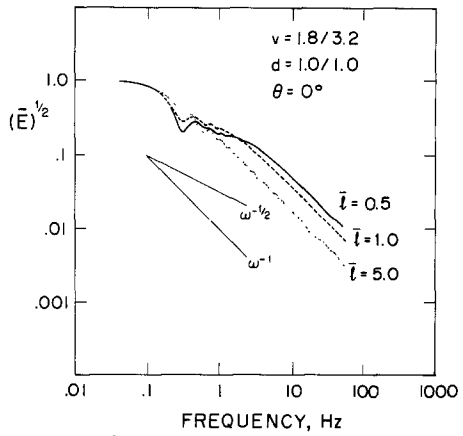

FIG. 9. The influence of coherence length on the mean spectrum for the fault with random variations of rupture velocity between 1.8 and 3.2 km/sec. Note the flattening of the spectrum due to the increase of the corner frequency associated with the coherence length.

completely satisfactory at azimuths of 90° and 180° (as expected), and is an adequate approximation at $\theta = 0°$ for the purpose of studying the general influence of various kinds of statistical rupture parameters on the radiated field.

Summary. The effect of coherent rupture propagation is to smooth the radiated waves and consequently reduce high frequencies. The effectiveness of the reduction depends on azimuth. For supersonic rupture, there is always an azimuth along which no destructive interference occurs ($\theta = 0°$ for $V = \beta$, $\theta = 90°$ for $V = \infty$).

The effect of incoherence is in general to increase high-frequency spectral amplitudes by adding a spectral corner, related to the coherence length, at higher frequencies than the corner due to the overall rupture length. The amount of increase depends on azimuth if the incoherence is due to variable rupture speeds, with virtually no increase at back azimuths but a large increase at forward azimuths. If, on the other hand, the incoherence is due to variable fault slip the increase is the same at all azimuths with the result that the ratio of spectra at various azimuths is similar to that produced by smooth coherent rupture.

Peak amplitudes. Although we have concentrated on the spectrum of the radiated energy, the Monte Carlo method can also be used to study peak amplitudes. As an

example, Figure 12a shows the dependence of the peak amplitudes of the wave forms in Figure 2 to variations in the mean rupture velocity. An ensemble of 20 runs was used to generate the results. The upper limit of rupture velocity was fixed at 3.2 km/sec, and the lower limit was decreased such that the mean velocity

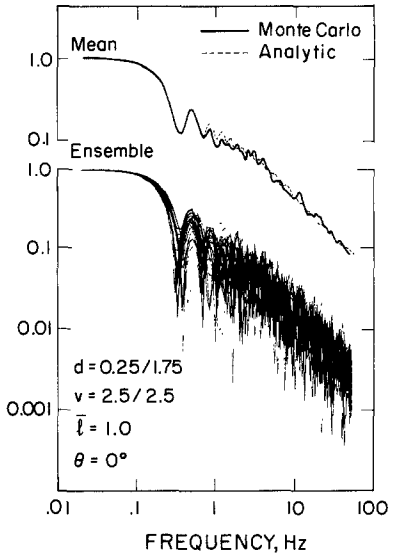

FIG. 10. Monte Carlo simulation of the spectra at a forward azimuth for the model with variable fault slip and constant rupture velocity. The lower set of curves show the 20 individual spectra comprising the ensemble. At the *top,* the mean spectrum of this ensemble (solid line) is compared with that computed from equation (A4).

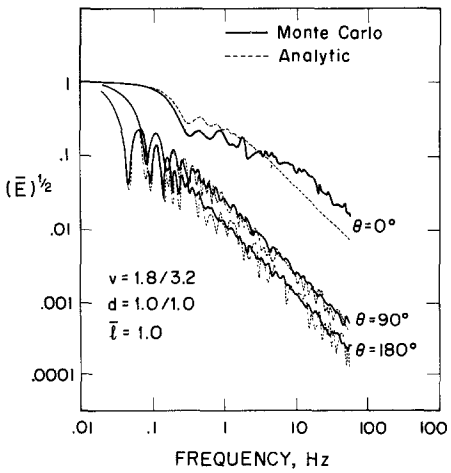

FIG. 11. Comparison of the mean spectra from the Monte Carlo simulations (solid lines) and the analytical formula (dashed lines) for the fault with variable rupture velocity and constant slip.

was lowered. For comparison, the dashed line shows the corresponding rupture velocity sensitivity of the peak motions for smooth rupture. The peak motions from the statistical model are similar to those predicted from a smooth rupture except at slow mean rupture velocities, where the peak motions are biased to high values by the fault segments with rupture velocities close to the shear velocity. A similar dependence of amplitudes on rupture velocity can be generated from the equations for $\bar{a}$ (Figure 12b). In this case $\bar{a}$ is the mean amplitude of the ground

displacement for the idealized fault model discussed earlier, not the mean of the peak amplitudes of the motion. In spite of the difference in definition, the sensitivity to rupture velocity is similar and suggests that the addition of randomness to the faulting process can lead to larger motions than would be produced by smooth rupture. This is contrary to the intuitive feeling sometimes encountered that the incoherence should decrease the peak motions. It must be remembered, however, that coherent rupture propagation leads to destructive interference. Any incoherence will tend to destroy this interference, with the result that spectral levels and peak motions will, in general, be larger than is the case of smooth rupture. It should be noted, as did Brune (1976), that the incoherence may come from variable wave propagation velocities in the fault zone rather than from variable rupture speed.

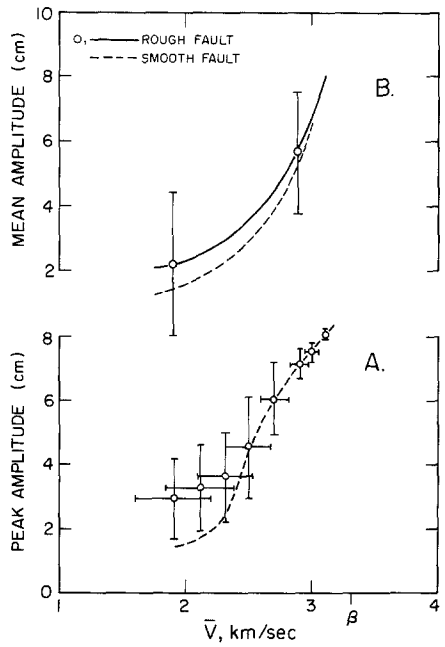

FIG. 12. Amplitudes as a function of mean rupture velocity. (A) Peak amplitudes, NS component of the instrument output for the model used in Figure 2 (southern segment), using a Monte Carlo simulation of 20 runs. Bars show 1 S.D. (B) Mean amplitudes for the types of wave form shown in Figure 5 (no instrument response), scaled by an arbitrary factor for comparison with (A). In each case the slip was constant and the rupture velocity varied between a fixed upper limit of 3.2 km/sec and a variable lower limit. In both (A) and (B) the results from the irregular faulting are compared with those from smooth rupture with properties equal to the mean of the irregular faulting parameters.

OTHER TYPES OF INCOHERENCE

The faulting discussed so far was deterministic in the sense that the rupture was unidirectional with a mean velocity, and the directivity effects expected for smooth rupture persisted even when randomness of the fault parameters was introduced. In order to neutralize the directivity effects it would seem that the assumption of unidirectional rupture with a monotonic sequence of triggering the adjacent fault segments must be abandoned. Going to the opposite extreme, we determined the mean spectrum for a fault in which rupture can occur randomly in space and time on the fault surface. This model is as close as we can come to purely random rupture. The resulting spectrum, given in Appendix B, is identical to the spectrum produced by instantaneous faulting with a ramp source-time function, and therefore directivity effects are still present, although the azimuthal differences are generally confined to a narrower range of angles than for unidirectional rupture. To completely

eliminate rupture directivity, it would be necessary to abandon not only unidirectional rupture, but also rupture on an extended planar surface.

For the discussion so far we assumed a step function for the time history of fault slip, but we expect finite rise times in reality. This will generally introduce a ω^{-1} decay in the spectrum, but if the particle displacement is jerky the effective corner beyond which the spectrum falls off at ω^{-1} may be at higher frequencies than expected for a smooth source-time function. The analysis of the effects on the spectra from a partially incoherent source-time function is similar to the derivation of the mean spectrum in equation (6), with the exception that directivity effects are not present since the rise time of a point on the fault as perceived at a station will not depend on azimuth.

The combination of randomness in the rupture propagation and in the source-time function can lead to a spectrum whose apparent high-frequency decay in the range of observational frequencies is less than the ω^{-3} decay given by most coherent source models (ω^{-1} from length, width, and rise time). Our statistical source model may then include the best features of the ω^{-3} model of Geller (1976), who included the effect of fault width, and the ω^{-2} model of Aki (1967), who did not, but who argues that the ω^{-3} model does not fit the data. The choice between the ω^{-2} and ω^{-3} models on the basis of data such as $M_s - m_b$ and $M_0 - M_s$ relations is, in our opinion, not resolved at this time, and we defer further discussion to a later paper dealing specifically with the implications of our model on teleseismic spectra.

Discussion

This paper was prompted by the sensitivity of near-fault motions to rupture velocity and azimuth found in a study of the 1906 San Francisco earthquake (Boore, 1977) in which simple, coherently propagating faults were used in the modeling. The question was whether similar effects would be predicted from more realistic, less coherent ruptures. The answer is yes, provided that the mean-rupture velocity is held constant. Mean-rupture velocity does play an important role, however, and if the mean-rupture velocity for a jerky rupture is less than predicted for a smooth rupture, the directivity effects may be reduced. For example, if rupture velocities for some small- to moderate-size ruptures have been found to be 0.9 β, the effective mean velocity from a longer rupture in the same region might be less than this if the rupture has to break through hard patches between segments. This brings up the question of how rupture properties are to be chosen for modeling of near-fault motions. We have seen here that the high-frequency motions of interest to engineers are sensitive to inhomogeneities in the fault parameters. There are few reliable estimates of mean rupture velocity, much less the statistical distribution of fault slip, rupture velocity, and coherence length. Modeling existing strong-motion records is one approach to estimating such parameters, but it is necessary to separate the effects of source and geology. We are in the process of such studies, using Monte Carlo simulations and restricting the data to rock sites, for which the ringing effects of local, low-velocity sediments should be minimized.

The models used in this paper were chosen for the ease with which the effects of incoherence could be studied. There are several reasonable changes to our models which can reduce the sentitivity of ground motions to rupture velocity and azimuth. First, if the waves propagate out of the perpendicular bisecting plane of the fault the cos θ/β term in equation (2) should be replaced by the apparent slowness of the wave in the direction of rupture propagation. This can reduce the effective Mach number. Second, we considered unidirectional faults only. While it seems to

be true that most large faults are predominately unidirectional, a small amount of bidirectional faulting can strongly influence the azimuthal dependence of the ground motions, especially at high frequencies. An example is given by the wave forms shown in Figure 2 for a model of the 1906 San Francisco earthquake. The evidence suggests that the significant faulting was predominantly unidirectional, rupturing away from the Lick Observatory station for about 300 km on the northern segment and toward the station for about 30 km on the southern segment (Bolt, 1968; Boore, 1977). The models show that because of directivity this rupture on the northern segment gives very small motions at Lick Observatory. Adding some bidirectionality to the faulting, by including a relatively short length of rupture toward the station on the southern segment, dramatically increases the predicted ground motions. As the period increases, however, the importance of the southern segment will decrease relative to that of the northern segment. The analysis we have made for unidirectional statistical rupture can be easily modified to account for bidirectional faulting.

As a final comment, although we are interested in the implications of incoherence at distances close to large faults, we have used two assumptions, for simplicity, that seem inconsistent with this desire. The first is that only far-field terms are considered. The second is that the solid angle subtended by the fault at the point of observation is small (this is needed in order to express the distance from any point on the fault to the receiver as a linear function of distance along the fault). We call this the point source approximation; it was necessary in the derivation of equation (2). The neglect of near-field terms and fault finiteness, however, are not crucial to our arguments. At the frequencies of interest we are almost always at least several wavelengths from the source and thus the near-field terms are of little importance. The finiteness effect certainly must be accounted for in any calculation of motions close to an extended fault, but this can be easily done by breaking the fault into a number of segments and using the point source approximation for each segment. This was done in the calculations presented in Figures 1 and 2, and we see that directivity effects are still present. Furthermore, Archuleta and Brune (1975) observed near-fault directivity effects in both laboratory and computer models. Thus, although the details of our results may depend on the finiteness of the fault, we expect our general conclusions to be valid.

ACKNOWLEDGMENTS

We benefited from numerous discussions with Henry Swanger and by his careful reading of the original manuscript. The research was supported by the Division of Advanced Environmental Research and Technology, National Science Foundation, Grant ENV75-05148.

APPENDIX A

Mean spectrum derivation. We can consider the time series of Figure 5 to be a random series $r(t)$ multiplied by a boxcar function $B(t; \Delta t_L)$, where Δt_L is the duration of the box. Following Blackman and Tukey (1958), the mean energy density spectrum $\bar{D}$, is given by

$$\bar{D}(\omega) = \frac{1}{2\pi} Q(\omega) * P(\omega) \tag{A1}$$

where $Q(\omega)$ = the square amplitude of the Fourier transform $B(t, \Delta t_L)$

$$Q(\omega) = \Delta t_L{}^2 \sin^2 \frac{\omega \Delta t_L}{2} \Big/ \left(\frac{\omega \Delta t_L}{2}\right)^2 \tag{A2}$$

and $P(\omega)$ is the mean power density spectrum of the random process $r(t)$. In our case, $r(t)$ is equivalent to the process given by random impact of particles in Brownian motion (Bendat, 1958). The autocovariance of this process is given by $\bar{a}^2 + \sigma_a{}^2 \exp(-\alpha|\tau|)$ where $\bar{a}$ = mean amplitude of the wave, $\sigma_a{}^2$ = variance of the amplitude, $\alpha^{-1} = \bar{t}$ = mean duration of each pulse, and the mean power spectrum is

$$P(\omega) = 2\pi\bar{a}^2\delta(\omega) + \frac{2\sigma_a{}^2\alpha}{\alpha^2 + \omega^2}. \tag{A3}$$

The convolution in (A1) can be performed analytically by using contour integration, giving the normalized energy density spectrum

$$\bar{E}(\omega) = \frac{\sin^2\omega\Delta t_L/2}{(\omega\Delta t_L/2)^2} + 2\left(\frac{\sigma_a}{\bar{a}\Delta t_L}\right)^2 (\omega^2 - \alpha^2 + \alpha(\omega^2 + \alpha^2)\Delta t_L - e^{-\alpha\Delta t_L}\{(\omega^2 - \alpha^2)\cos\omega\Delta t_L + 2\alpha\omega\sin\omega\Delta t_L\})/(\omega^2 + \alpha^2)^2 \tag{A4}$$

where $\bar{D} = (a\Delta t_L)^2\bar{E}$. When $\alpha\Delta t_L$ is large (A4) reduces to equation (6) in the text.

The exact expression (A4) was actually used in the computations presented in Figures 7 through 9 rather than the approximate expression (6). It will be noted that the term on the right-hand side of equation (A4), representing the contribution of the random component of the source, does not vanish at zero frequency as one would expect. This is a simple consequence of the fact that (A4) leads to a root mean-square spectrum, rather than a mean spectrum. The problem is not critical and is easily side-stepped by normalizing all spectra to the value at zero frequency.

APPENDIX B

Completely random fault. Consider a fault broken into N subfaults, each of moment M_0/N where M_0 is the total fault moment. Let the dimensions of each subfault be small enough that the radiation in the frequency range of interest be equivalent to that of a point source. The radiation from the ith subfault will then be

$$u_i(t) = (C/N)\,\delta(t^* - \tau_i + \xi_i\cos\theta/\beta) \tag{B1}$$

where C is a constant depending on azimuth, moment, and mean distance from the fault [see equation (3) in the text], and $t^* = t - r_0/\beta$ = reduced travel time. We allow the subfault, located at the random position ξ_i to radiate at the random time τ_i. We can form a new random variable η_i by

$$\eta_i = \tau_i - \xi_i\frac{\cos\theta}{\beta}. \tag{B2}$$

The total motion is then given by

$$u(t) = C\frac{1}{N}\sum_{i=1}^{N}\delta(t^* - \eta_i) \tag{B3}$$

and the squared amplitude spectrum is

$$|U^2(\omega)| = C^2\frac{1}{N^2}\left\{\left(\sum_{i=1}^{N}\cos\omega\eta_i\right)^2 + \left(\sum_{i=1}^{N}\sin\omega\eta_i\right)^2\right\}. \tag{B4}$$

With the definitions

$$X = \cos \omega \eta_i$$

$$Y = \sin \omega \eta_i$$

we see that (B4) is proportional to the square distance from the origin after N steps of uniform length, but random direction. This is a two-dimensional random walk. It is straightforward (Middleton, 1960) to show that the expected value $E(|U(\omega)|^2)$ is given by

$$E(|U(\omega)|^2) = C^2 \frac{1}{N^2} \{N[E(X^2) + E(Y^2)] + (N^2 - N)[E^2(X) + E^2(Y)]\} \quad \text{(B5)}$$

which for large N reduces to

$$E(|U(\omega)|^2) = C^2\{E^2(X) + E^2(Y)\} \quad \text{(B6)}$$

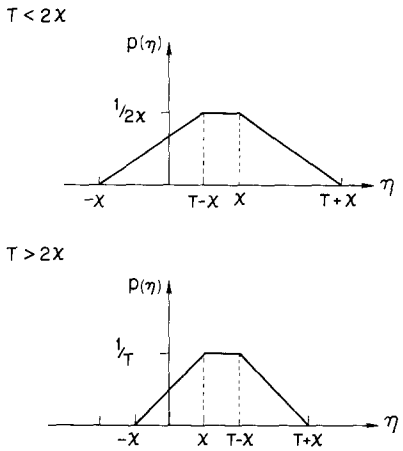

FIG. 13. Probability distribution function of η, used in Appendix B, where $\chi = L \cos \theta/(2\beta)$. The function used depends on the relative size of T and χ.

where the expected values of X and Y are given by the integrals

$$E(X) = \int \cos \omega \eta p(\eta) d\eta$$

$$E(Y) = \int \sin \omega \nu p(\eta) d\eta \quad \text{(B7)}$$

where $p(\eta)$ = probability density function (*pdf*) of η, derived from the *pdf*'s of τ and ξ. The latter *pdf*'s were assumed to be rectangular between 0 and T and $-L/2$ and $L/2$, respectively (where L = fault length). $p(\eta)$ is sketched in Figure 13. E represents the expected value, and not the energy density spectrum as in Appendix A. Doing the integrals in (B7) leads to the particularly simple result for the mean spectrum

$$|\overline{U(\omega)}| \equiv (E(|U(\omega)|^2))^{1/2} = \frac{|\cos 2\theta|}{4\pi\rho\beta^3} \frac{M_0}{r} \left| \frac{\sin \omega\chi}{\omega\chi} \right| \left| \frac{\sin \omega T/2}{\omega T/2} \right| \quad \text{(B8)}$$

where $\chi = L \cos \theta/2\beta$. As might be expected on intuitive grounds, this spectrum also

corresponds to a fault with infinite rupture velocity and a ramp source time function of duration T [see equations (1) and (4) in the text].

References

Aki, K. (1967). Scaling law of seismic spectrum, *J. Geophys. Res.* **72,** 1217–1231.

Aki, K. (1972). Scaling law of earthquake source time-function, *Geophys. J.* **31,** 3–25.

Ang, A. HS. and W. H. Tang (1975). *Probability Concepts in Engineering Planning and Design, vol. I: Basic Principles*, John Wiley & Sons, Inc., New York.

Archuleta, R. J. and J. N. Brune (1975). Surface strong motion associated with a stick-slip event in a foam rubber model of earthquakes, *Bull. Seism. Soc. Am.* **65,** 1059–1071.

Bendat, J. S. (1958). *Principles and Applications of Random Noise Theory*, John Wiley & Sons, Inc., New York.

Benioff, H. (1955). Mechanism and strain characteristics of the White Wolf fault as indicated by the aftershock sequence, in *Earthquakes in Kern County California during 1955*, G. B. Oakeshott, Editor, Calif. Div. Mines Bull. 171, 199–202.

Ben-Menahem, A. (1961). Radiation of seismic surface waves from finite moving sources, *Bull. Seism. Soc. Am.* **51,** 401–435.

Blackman, R. B. and J. W. Tukey (1958). *The Measurement of Power Spectra*, p. 93, Dover Publ., Inc., New York.

Blandford, R. R. (1975). A source theory for complex earthquakes, *Bull. Seism. Soc. Am.* **65,** 1385–1405.

Bolt, B. A. (1968). The focus of the 1906 California earthquake, *Bull. Seism. Soc. Am.* **58,** 457–471.

Boore, D. M. (1977). Strong-motion recordings of the California earthquake of April 18, 1906, *Bull. Seism. Soc. Am.* **67,** 561–577.

Boore, D. M. and D. J. Stierman (1976). Source parameters of the Pt. Mugu California earthquake of February 21, 1973, *Bull. Seism. Soc. Am.* **66,** 385–404.

Brune, J. N. (1976). The physics of earthquake strong motion, in *Seismic Risk and Engineering Decisions* ch. 5, 140–177, C. Lomnitz and E. Rosenbleuth, Editors, Elsevier Scientific Publ. Co., Amsterdam.

Das, S. and K. Aki (1977). Fault plane with barriers: a versatile earthquake model, *J. Geophys. Res.* **82,** 5658–5670.

Geller, R. J. (1976). Scaling relations for earthquake source parameters and magnitudes, *Bull. Seism. Soc. Am.* **66,** 1501–1523.

Hanks, T. C. (1972). A contribution to the determination and interpretation of seismic source parameters, *Ph.D. Thesis*, 126–134, Calif. Inst. of Tech., Pasadena.

Haskell, N. R. (1964). Total energy and energy spectral density of elastic wave radiation from propagating faults, *Bull. Seism. Soc. Am.* **54,** 1811–1841.

Haskell, N. R. (1966). Total energy and energy spectral density of elastic wave radiation from propagating faults. Part II. A statistical source model, *Bull. Seism. Soc. Am.* **56,** 125–140.

Madariaga, R. (1977). High frequency radiation from crack (stress drop) models of earthquake faulting *Geophys. J.* **51,** 625–651.

Middleton, D. (1960). *An Introduction to Statistical Communication Theory*, p. 359, McGraw Hill Book Co., Inc., New York.

Nur, A. (1978). Nonuniform friction as a physical basis for earthquake mechanics: a review *Pure Appl. Geophys.* (in press).

Savage, J. C. (1966). Radiation from a realistic model of faulting, *Bull. Seism. Soc. Am.* **56,** 577–592.

Savage, J. C. (1971). Radiation from supersonic faulting, *Bull. Seism. Soc. Am.* **61,** 1009–1012.

Department of Geophysics
Stanford University
Stanford, California 94305 (D.M.B.)

U.S. Geological Survey
345 Middlefield Road
Menlo Park, California 94025 (W.B.J.)

Manuscript received August 10, 1977